Plasma Physics and Controlled Fusion Vol.28, No.9A pp.1413-1428, 1986 0741-3335/86$3.00+ .00
Printed in Great Britain Institute of Physics and Pergamon Journals Ltd.

PROPERTIES, CONTROL AND ICR-HEATING OF THE PLASMA IN TEXTOR

G.H. Wolf, H.L. Bay, G. Bertschinger, W. Bieger[1], P. Bogen, W. Brüssau, G.A. Campbell[2], Y. Cao[3], R.W. Conn[2], K.H. Dippel, H.G. Esser, K.H. Finken, G. Fuchs, B. Giesen, D.M. Goebel[2], E. Graffmann, H. Hartwig, E. Hintz, F. Hoenen, K. Höthker, A. Kaleck, H. Kever, L. Könen, M. Korten, L. Li[3], Y.T. Lie, W.K. Leung[2], A.E. Pontau[4], A. Pospieszczyk, D. Reiter, A. Rogister, G. Ross[5], D. Rusbüldt, U. Samm, B. Schweer, J. Schlüter, H. Soltwisch, W. Stodiek[6], G. Thomas[4], F. Waelbroeck, G. Waidmann, P. Wienhold, J. Winter, R. Yamauchi[7]

Institut für Plasmaphysik, Kernforschungsanlage Jülich GmbH, Association EURATOM-KFA, D-5170 Jülich, FRG

[1]Fachhochschule Jülich, D-5170 Jülich, FRG. [2]University of California at Los Angeles, USA. [3]Institute of Plasma Physics, Academia Sinica, Hefei, The People's Republic of China. [4]Sandia National Laboratories, Livermore, USA. [5]INRS-ENERGIE, Varennes, Quebec, Canada. [6]Princeton Plasma Physics Laboratory, USA. [7]JAERI, Tokai, Japan

and

T. Delvigne, P. Descamps, F. Durodié, M. Jadoul, R. Koch, D. Lebeau, A.M. Messiaen+, D.I.C. Pearson, P.E. Vandenplas, R. Van Nieuwenhove, G. Van Oost, G. Van Wassenhove, R.R. Weynants+

Plasma Physics Laboratory, Ecole Militaire/Koniklijke Militaire School, Association EURATOM-Belgian State, B-1040 Brussels

+Senior research associate at the NFSR, Belgium

ABSTRACT

The accessible parameter range, the impurity contents and the susceptibility to ICRH power input depend on conditioning procedures and on the surface materials of limiter and liner. The respective combinations stainless steel and inconel, "carbonized" stainless steel and "carbonized" inconel as well as "carbonized" graphite and "carbonized" inconel have been compared. For the latter pulses of up to 3.8 sec duration and loop voltages below 1 V could be achieved and the accessible operation regime in the Hugill-Diagramme could be significantly extended. The metal concentrations were reduced to the order of 10^{-5}, whereas the total concentration of carbon and oxygen impurities was typically around two to three percent, with a falling tendency in the course of repetitive baking treatments.

Results on j(r) derived from polarimetry are presented and discussed: in many cases the stationary value of q(0) was found to be $\gtrsim$ 30 % below unity. No sawteeth on the j(r) profile could be observed.

ICR heating has been extended to the 2 MW level and to the minority/second harmonic mode. The τ_E-scaling still remains comparable to that of the L-regime. With the Ansatz $E = \tau_{OH}P'_{OH} + \tau_{AUX}P_{RF}$ the best fit gives $\tau_{AUX}[ms] = (60\pm15)I_p[MA]$. The degradation of τ_p is similar to that of τ_E; the fluxes of neutral hydrogen, carbon and oxygen and the value of n_e close to the limiter increase with the RF power. Pronounced sawteeth are observed in the H_α-signal at the main limiter and at the wall and also in n_e close to the limiter with amplitudes of up to 50 %.

The application of ICRH increases the particle removal by the pump limiter ALT-I as a consequence of the reduced τ_p and the resulting increased plasma flux into the entrance throat. This effect compensates potential difficulties for pump limiter application from the heat load on the limiter head which was found to increase more than linearly with P_{RF}. First experiments with localized perturbation coils for boundary "ergodization" resulted in a pronounced stationary island pattern in the boundary layer; they influenced the global plasma confinement and, in some cases, led to a quench of the internal m=2 mode.

GENERAL PLASMA PROPERTIES AND CARBONIZATION

The TEXTOR research programme /1/ focusses on the systematic analysis of plasma wall interaction, the development of a suitable wall system and the production of quasi-stationary long-pulse high-temperature plasmas with tolerable impurity concentrations, with well-defined boundary layer and with relevant particle and power fluxes through the boundary.

First, the present paper describes the method of wall carbonization developed in Jülich /2-5/ and some characteristic features of the TEXTOR plasma /6/ obtained with this method for both, metal limiters and graphite limiters. Moreover, the effect of ICRH heating (2MW, 1 sec) /7,8/ on plasma parameters and on the boundary layer /9,10/ is discussed, together with the application of the single head pump limiter ALT-I /11-13/ and of the localized set of magnetic perturbation coils for boundary "ergodization" /14-16/.

Originally, TEXTOR had been operated with an inconel liner and with a system of stainless steel limiters /17/. Under these conditions, the plasma discharges were characterized by concentrations of metallic impurities - depending on n_e - of up to several 10^{-4} and of a disruption limited tolerable ICRH power limit of only 100 to 200 kW /18/. The plasma-chemical deposition of carbon on the first wall has been developed for TEXTOR in order to suppress the production of metallic impurities and to achieve a satisfactory susceptibility of the plasma to powerful long-pulse ICRH heating. It may be recalled that until recently the method of impurity control - in limiter Tokamaks - generally consisted of the use of (i) graphite limiters (and protection plates), (ii) metal walls and (iii) Ti- or Cr-gettering in particular in order to reduce the oxygen concentration. This procedure had the disadvantage that in the course of Tokamak operation the graphite limiters became increasingly contaminated by the redeposition of metallic wall material which also led to a steady increase of the metal impurity concentration in the plasma core.

Carbonization suppresses this mechanism. Carbonization is the plasma-chemical coating of the whole wall system with a sufficiently thick (i.e. several hundred monolayers) amorphous carbon layer of a relative hydrogen (deuterium) content of about 0.4.
This layer can be applied by a specific radio-frequency assisted glow discharge in an adjustable mixture of e.g. D_2/CD_4. Any desired ratio between the H and D composition of the plasma can be obtained. The method is well-defined and reproducible. By means of appropriate glow-discharge cleaning the coating can also be completely removed.

First, carbonization has been applied upon the above mentioned all metal wall system. The success of this method led to a reduction of the metal concentration in the plasma core towards the 10^{-5} regime and to the possibility of coupling ICRH power (with the same antenna system) in the MW-regime. Erosion of the carbonization layer on the exposed parts of the limiters, however, led to the need for some recarbonization after about 100 discharges. Moreover, stainless steel as the bulk material of the limiters is not considered suitable to accept high power fluxes, e.g. on the leading edges.

Therefore, the material of the limiter system, i.e. of the movable main limiters, of the antenna protection limiters and of the inboard limiter (mainly for protection against disruptions), has been changed over from stainless steel to graphite during the last summer break. Initially, this led to a pronounced prolongation of the operational period until recarbonization is required. However, as compared to the carbonized metal system, there is now an even more apparent source-sink behaviour of the limiter system with respect to the hydrogen balance, and the C and/or O concentration is roughly twice that as obtained before: the latter depends strongly on the application of intense baking after which a significant reduction of the C and/or O content can be achieved. A comparison between these cases is given in Table 1 which, among others, shows Z_{eff} from soft X-ray measurements (under the assumption of equal C and O concentration). Since in the course of TEXTOR operation some metal erosion has occurred e.g. from diagnostic probes, we observed also some metallic contamination of the graphite limiters: this led to recarbonization requirements which are comparable to the situation with carbonized metal limiters.
From a systematic study of parametric dependences, a further comparison is comprised by the "Hugill-Diagramme" for these three cases which essentially shows that both, the q-limit and the density limit could be significantly shifted after carbonization had been applied: this holds for both limiter materials, stainless steel and graphite. The present density limit with OH-discharges at 2.0 T lies at $\bar{n}_e = 5.3 \times 10^{13} cm^{-3}$ (with ICRH it could be shifted to

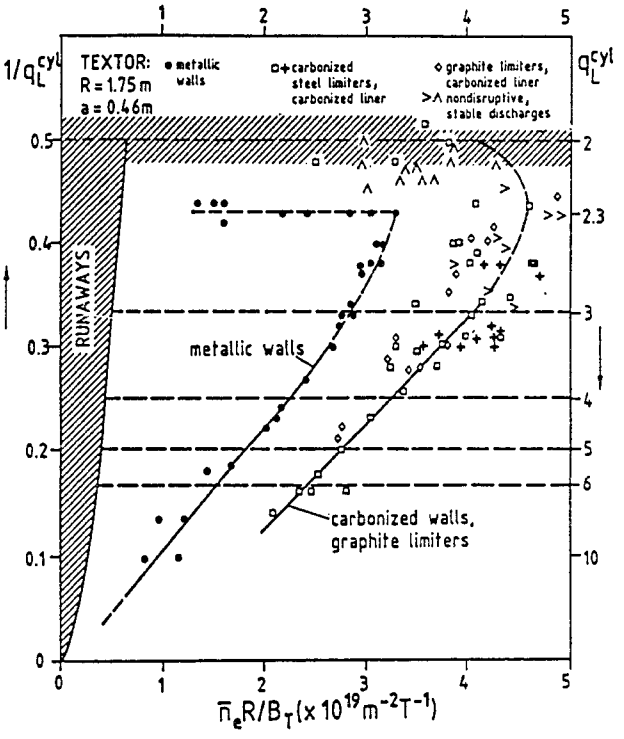

Fig. 1. Operational regime of OH-discharges for metallic limiters and walls •, for carbonized metallic limiters and walls □+, and for carbonized graphite limiters and (metallic) walls ◇>^ ($B_T \leq 2.0$ T, $I_p \leq 540$ kA).

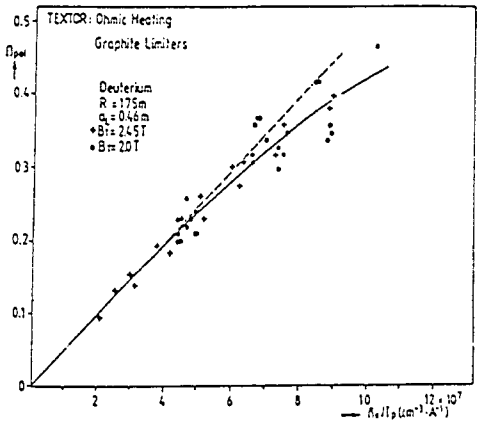

Fig. 2. β_{pol} vs. $\bar{n}_e/I_p$ scaling for carbonized graphite limiters and (metallic) walls.

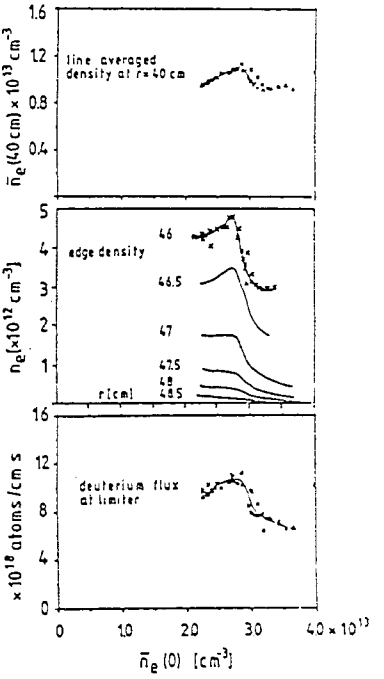

Fig. 3. Variation of density and of particle flux as a function of central line averaged density $\bar{n}_e$ for OH discharges and for carbonized graphite limiters and (metallic) walls.

$5.7 \times 10^{13} cm^{-3}$). The corresponding Murakami parameter which has now been achieved under OH-conditions is

$$M = \bar{n}_e \frac{R_o}{B_T} = 4.9 \times 10^{19} \left[T^{-1}\, m^{-2}\right].$$

The above mentioned parameter scans permitted to establish - for $\bar{n}_e$ between 1×10^{13} and 5×10^{13} cm^{-3} and for I_p between 340 kA and 500 kA - a scaling of β_{pol}:

$$\beta_{pol} = 4.8 \times 10^{-9}\, \bar{n}_e / I_p \qquad \text{with} \qquad I_p[A],\ n_e[cm^{-3}],$$

which is shown in Fig. 2. The overall pulse duration of the discharges in this density range could be extended to 3.8 sec; for B_T = 2.0 T the value of I_p could be increased to 540 kA and τ_E reached 100 ms. Upgrading of the TEXTOR machine permits now to extend B_T up to 2.6 T or even slightly beyond.

At higher densities, a broadening of the boundary layer, accompanied by increased luminosity, could be visually observed by use of a (tangentially viewing) TV-camera. Detailed measurements in the boundary have shown that, for $\bar{n}_e \gtrsim 3 \times 10^{13} cm^{-3}$, the plasma starts to become detached from the limiter resulting in reduced fluxes, density and heat loads there /10/ as can be seen in Fig. 3.

	without	with carbonization	
	inconel liner steel limiters a)	inconel liner steel limiters b)	inconel liner graphite limiters c)
$Z_{eff}(0)$	3.2	1.6(1.2)	2.0
$\bar{n}_e$	$4.2 \times 10^{13} cm^{-3}$	$4.6 \times 10^{13} cm^{-3}$	$5.3 \times 10^{13} cm^{-3}$
Oxygen	3×10^{-2}	$6 \times 10^{-3} (2 \times 10^{-3})$	1×10^{-2}
Carbon		$6 \times 10^{-3} (2 \times 10^{-3})$	1×10^{-2}
Iron	5×10^{-4}	$2 \times 10^{-5} (\lesssim 10^{-5})$	2×10^{-5}

TABLE I. Typical composition of a deuterium plasma for various wall conditions. Best values ever achieved for b) in brackets. Impurity figures are relative concentrations on the axis. The carbon and oxygen values in b) and c) are evaluated under the assumption of equal concentration.

CURRENT DENSITY PROFILES

The poloidal magnetic field distribution in TEXTOR has been determined by probing the plasma with an array of HCN laser beams measuring the Faraday rotation of their planes of polarization and the phase shifts caused by the electron density /19/. The data analysis is based on the assumption of eccentric circular flux surfaces in accordance with numerical equilibrium calculations. The total error of the resulting current density profile is estimated to be about ± 5 % to ± 10 % at half the plasma radius. For the central current density an accuracy of ± 15 % to ± 20 % is achieved by slowly moving the plasma across the probe beams and thereby virtually multiplying the number of chords /20/. The agreement between the positions of the q=1 surface as determined by the Faraday rotation measurements and by temperature and density sawteeth confirms the absence of systematic errors. Temporal evolutions of the current density profiles have been determined for discharges with various magnitude and time dependen-

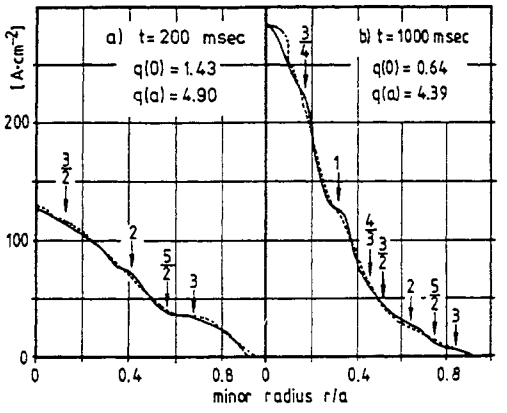

Fig. 4. Time development of the j profile for the times of a) 200 and b) 1000 msec. q (0) develops from 1.4 to 0.64. The dashed line gives the measured values, whereas the solid line represents computed stable profiles (except for m = 1).

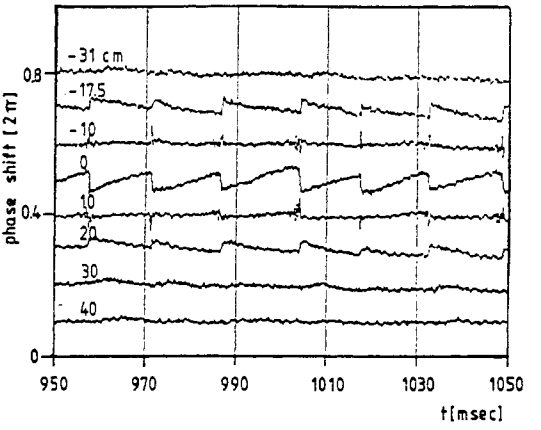

Fig. 5. Sawtooth relaxations of line integrated electron densities for the case of Fig. 4. The numbers give the positions of the probe beams relative to R_o = 175 cm.

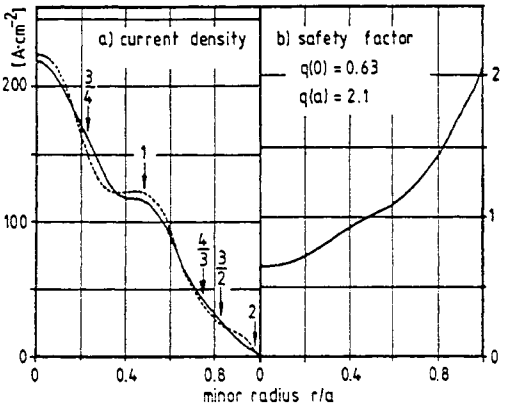

Fig. 6. a) Current density and b) q profile with large q = 1 surface of a discharge which is first stable and then violently develops a m=1 mode seen in Fig. 7.

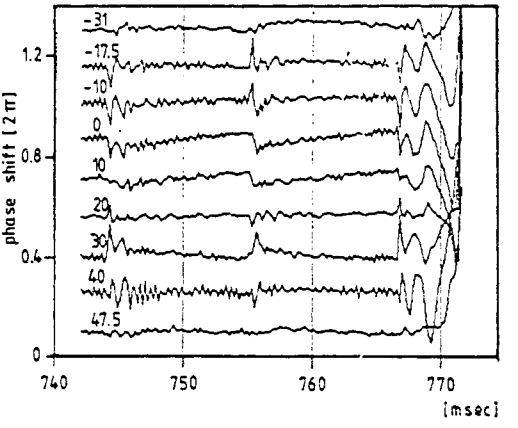

Fig. 7. Sawtooth behaviour of line integrated densities for the case of Fig. 6 showing the m = 1 mode at 767 msec which leads to a termination of the discharge.

ces of plasma current and toroidal field, and these have been compared with linear tearing mode stability theory using a cylindrical delta prime programme (kindly provided by K. Lackner, Garching).

In all cases marginally stable profiles could be generated for all modes with m=1 which coincide with the measured profiles within the experimental accuracy. The m=1 case is predicted unstable for all conditions with q on axis less than 1. It is thus surprising to observe that (as seen in Fig. 4) the current distribution develops in time with q(0) going from 1.4 at 200 msec down to 0.64 at 1000 msec without leading (necessarily) to a large m=1 internal kink instability, which would depress the current density profile by reconnection to q(0)=1. Sawtooth activity is nevertheles observed in such cases (Fig. 5) flattening the temperature and density profiles, but apparently not the current density profile.

For this situation we conclude that the sawtooth activity, especially under the persistent condition of q(0) significantly less than 1, cannot be the result of a complete reconnection process involving the m=1 internal kink mode, because of the impossibility of recovery of low q on axis between sawtooth relaxations /21/.

However, the generally predicted rapid growth of the m=1 internal kink for the case of q(0) about 0.6 has also been observed (Fig. 6). After more than 0.5 sec during which the current distribution has shown a fairly stationary behaviour with only small density sawteeth (Fig.7), a large m=1 mode develops, and the observed negative voltage spike indicates a large poloidal flux change. Eventually, this leads to a termination of the discharge. These phenomena would be difficult to understand with the assumption of q(0) near 1.

Conditions under which the resistive m=1 mode may be marginally stable are not known theoretically for q on axis significantly less than 1 and are now being investigated /22/.

ION CYCLOTRON HEATING AND RESULTING EFFECTS

Introduction

The principal features of the previous ICRH results on TEXTOR have been reported in /23/ and /7/. The most important changes for the conditions of the ICRH operation reported here are: 1) the use of main and antenna limiters made of graphite to replace the previous stainless steel ones; 2) the use of identical top and bottom antennae /24/ with central conductors of the broad type (mean width: 17 cm); 3) the use of low minority concentrations in a D-(H) plasma (N_H/N_D < 1 %), instead of the previous mode conversion regime.

With these changes the general characteristics of the results remain the same as those reported in /7/. Long pulse (~ 1s), low impurity ICRH with stationary plasma parameters has been obtained but now with an RF power fed to the antenna P_A which has reached 2.3 MW. Given an antenna loss of 180 KW, about 92 % of this value contributes to P_{RF}, the power effectively radiated into the machine, yielding a total power coupled to the plasma $P_{tot} = P_{RF} + P'_{OH}$ of 2.5 MW, which is 6.3 times the remaining OH power P'_{OH} at a plasma current I_p = 500 kA, which causes also a lengthening of the current flat-top by means of the resulting Vs saving. An adequate wall carbonization is also mandatory to bring up the power at the MW level without plasma disruption or antenna breakdown. This consists of glow discharge in a mixture of D_2 and CD_4, in order to reach the low H isotopic content in the tokamak discharge, and is followed by a baking of the C-limiters to avoid a large gas release during ICRH. The results reported here correspond to I_p = 0.48 - 0.50 MA, B_0 = 1.9 - 2.0 T and a main limiter radius of 0.46 m.

Results pertaining to a typical 2 MW shot are shown in Fig. 8: a) Temporal evolution of the total plasma energy content. E_{dia} is measured by diamagnetism and E_{equ} (dotted line curve) is computed from an equilibrium code using the measured vertical field and the current density profile as input data. The kinetic energy content E_{kin} as computed from the electron density and temperature profiles, the central ion temperature T_{io}, and assuming the same ion temperature profile as for the electrons leads to a value ~ 20 % lower. b) Temporal behaviour of the total number of electrons N_e in the discharge as obtained from HCN interferometry. c) The central electron energy density $E_{eo} = 3/2\, n_{eo} T_{eo}$ computed from the ECE signal from T_{eo} and the Abel inverted HCN data for the central density n_{eo}. d) The central ion temperature T_{io},

in a solid line, as obtained from the neutron yield. The dotted line shows for comparison $T_{io,A}$ as computed from equipartition alone (Artsimovitch law) using n_{eo} and T_{eo} as input data. The larger value of $T_{io,neutron}$ with respect to the equipartition value in the ICRH part of the shot is attributed to direct RF heating of the ions. e) The current profile parameter α_j /25/ obtained from the HCN polarimetric data using the following approximate relation for the current density profile $j = jo\ Ro/R\ [(1 - r^2/a^2)^{\alpha_j} - \mathcal{E}(r)\ (R-Ro)/R]$ with $|\mathcal{E}(r)| < 0.5$.

A large broadening of the density profile occurs during ICRH (see Fig. 9c), whereas no change or, at most, a slight flattening of the j-profile is observed.

Energy and Global Energy Confinement Time Scaling

The energy increase appearing during ICRH is always partly due to an increase in density (as reflected by N_e on Fig. 8b) and changes in its profile. In order to decouple the effect of density increase from the effect of the total power coupled to the plasma P_{tot} on the energy content E and resulting global energy confinement time $\tau_E = E/P_{tot}$, a careful selection of shots has been made with the same central chord density $\bar{n}_e$ for various values of P_{tot} (power scan) or the same P_{tot} and various $\bar{n}_e$ (density scan). To minimize the scatter in the experimental points these have been chosen from the same series of shots. The results are shown in Fig. 9a for the power scan and in Fig. 10 for the density scan. The conservative value of $E = E_{dia}/1.2 = E_{kin}$ is taken. As for the mode conversion regime analysis /2/, the results pertain to an L-mode type scaling which is found in agreement with either: (i) the Kaye-Goldston scaling /26/ expressed as $E_{K-G}(kJ) = 0.02\ \bar{n}_e^{0.26}\ P_{tot}^{0.42}\ I_p^{1.24}$ (10^{13} cm^{-3}, MW, kA) and valid for $P_{tot} > 3\ P'_{OH}$; this has a vanishing value of τ_E for large P_{tot}, or: (ii) a less pessimistic scaling law using an asymptotic, non-zero auxiliary heating confinement time $\tau_{AUX} = (\Delta E)_{RF}/P_{RF}$ to which τ_E reduces when $P_{RF} \gg P'_{OH}$.

As in Ref. /7/ we take

$$E = \tau_{OH}\ P'_{OH} + \tau_{AUX}\ P_{RF} \qquad (1)$$

assuming that τ_{OH} is the OH confinement time taken at the (constant) n_{eo} reached during RF and for the given machine parameters (B_t, I_p, R_o, a). For the power range and the plasma parameters considered in Fig. 9, a good fit for the dependence of P'_{OH} on P_{RF} is given by $P'_{OH} = P_{OH} - \delta P_{RF}$ with $\delta = 0.1$. This value of δ is also roughly in agreement with the expectation from Spitzer resistivity and the observed mean T_e increase shown in Fig. 11. Introducing P'_{OH} in Eq (1) one obtains the linear law $E = A + BP_{tot}$ shown in Fig. 9a. The dependence of B on τ_{AUX} is expressed by $B \cong dE/dP_{tot} = (\tau_{OH}\ dP'_{OH}/dP_{RF} + \tau_{AUX})(dP_{tot}/dP_{RF})^{-1}$.

The corresponding mean value of τ_{AUX} = 24 ms together with the values of τ_{AUX} derived from Eq. (1) for each experimental point are also indicated in Fig. 9b.

The results pertaining to the density scan are shown in Fig. 10. The OH curve ($P_{tot} = P_{OH} = 0.6$ MW) reflects the neo-Alcator behaviour of TEXTOR as expressed by Eq. (7) of Ref. /7/. It appears that the increase of τ_E with $\bar{n}_e$ becomes less and less pronounced as P_{tot} increases and that the asymptotic value for $P_{RF} \gg P'_{OH}$ expressed by τ_{AUX}, computed from Eq. (1), has practically no longer a dependence on density. This behaviour is similar to that observed with NBI in ASDEX /27/. We also note: (i) that the change of τ_E from the OH to the ICRH phase of a shot depends on the chord densities $\bar{n}_e$ achieved in OH and during ICRH; the arrows in Fig. 10 show typical trajectories during single shots starting from the OH and ending at the ICRH representative point. The τ_E degradation observed during a shot is thus particularly sensitive to the $\bar{n}_e$-evolution; (ii) Fig. 10 suggests that no τ_E degradation occurs at relatively low densities $\bar{n}_e = 1.5 \times 10^{13}$cm^{-3}. The direct confirmation of such a behaviour was not possible due to the lack of sufficient control of the density rise during high power ICRH. As shown in Fig. 12a and discussed below the particle confinement time τ_p undergoes a similar degradation to that of τ_E as P_{tot} is increased.

We may conclude that, although the total power has been extended up to 2.5 MW, i.e. $6.3 \times P'_{OH}$, it is still not yet possible to rule out a Kaye-Goldston τ_E scaling but, on the other hand, the results are consistent with a non vanishing τ_{AUX}. Comparing the results of Ref. /7/ with these, it appears that the value of τ_E obtained with low minority concentration is similar or slightly lower than observed with mode conversion. All the results are compatible with the scaling law of Eq. (1) choosing $\tau_{AUX}(ms) = (60 \pm 15)\ I_p(MA)$.

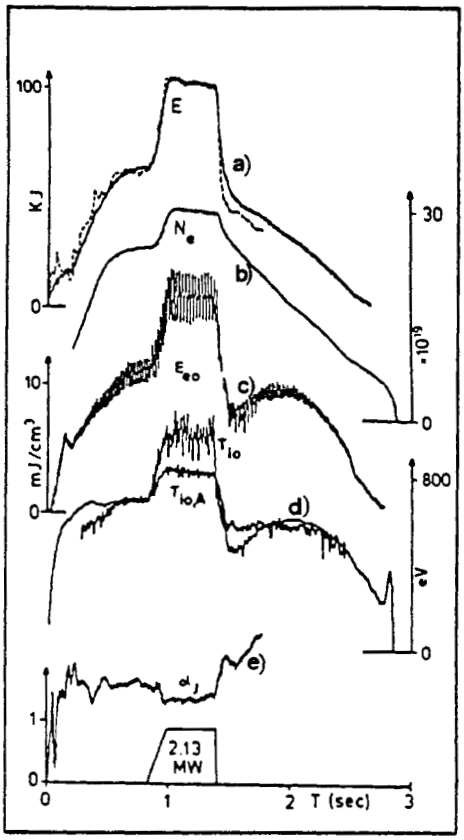

Fig. 8. Time evolution of various plasma parameters during an ICRH heated shot(#19161). a) E is the plasma energy content (solid line E_{dia}, dotted line E_{equ}) , b) N_e ; c) $E_{eo} = 1.5\, n_{eo}T_{eo}$ is the central electron energy density ; d) Central ion temperature (i)T_{io} measured from neutron emission (ii) $T_{io,A}$ computed from equipartition ; e) Current profile parameter α_j.

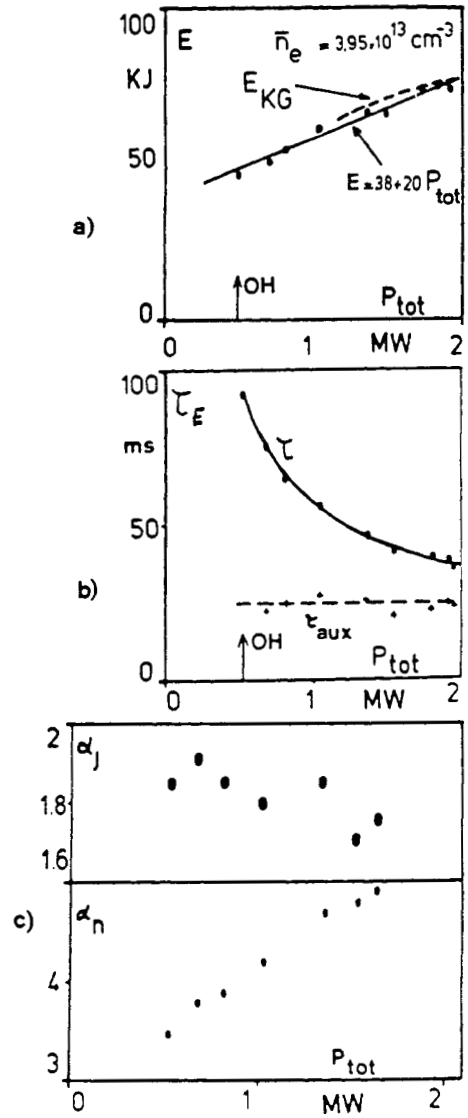

Fig. 9. Power scan results (at constant $\bar{n}_e = 3.95 \times 10^{13}$cm^{-3}; shots # 19513-19537). a) Plasma energy content as compared with the Kaye-Coldston scaling(dotted line) and the scaling of Eq. (1) (solid line) ; b) Global confinement time τ_E with the corresponding values of τ_{AUX} calculated from Eq. (1) ; c) Corresponding variation of the current profile parameter α_j and the density profile parameter α_n.

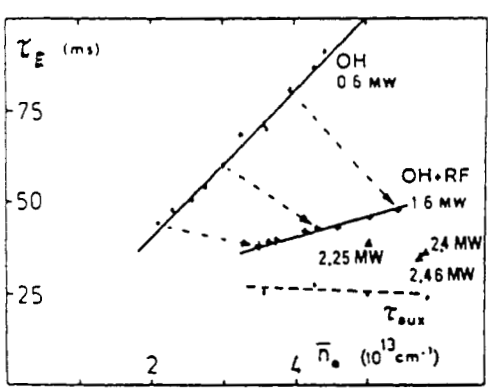

Fig. 10. Density scan evolution of τ_E at constant values of P_{tot} = 0.6 MW (OH only), P_{tot} = 1.6 MW, ≃ 2.4 MW(OH + ICRH) and derived values of τ_{AUX}. The arrows indicate the evolution from the OH to the ICRH phases in particular shots (# 18940-18947, 19161, 20349, 20351).

Heating Results and Profile Consistency

The observed increases in central temperatures T_{eo} (ECE) and T_{io} (neutrons) during the power scan experiment of Fig. 9 are shown, versus P_{RF}, in Fig. 11. The value of T_{io} due only to energy equipartition, as predicted from the above-mentioned Artsimovitch law, is also indicated. When comparing these results with the corresponding mode conversion case (see Fig. 6 of Ref. /7/), it is seen that there is less electron heating and more ion heating for the present low minority concentration experiments. A summary of the comparison is given in Table 2. The central RF power densities coupled to the electrons $p_{RF,e}$ and to the ions $p_{RF,i}$, as obtained from the central power density balance (see § 4.2 of Ref. /7/), has a similar increase of $p_{RF,i}$ with respect to $p_{RF,e}$ in the present experiments, as also shown in Table 2. From Fig. 11, it appears also that the electrons loose less power and the ions gain less by equipartition in this regime. The smaller relative increase of the central electron energy density E_{eo} as compared to the total energy increase (compare OH and ICRH phases on Fig. 8a and c) is attributable partly to the fact that ions are, relatively speaking, heated more than electrons and partly to the broadening of the density profile.

As shown on Figs. 8e and 9c and already stated at lower P_{RF} in Ref. /7/ there exists only a slight tendency towards broadening of the current profile with RF power even if the total power fed to the plasma changes by a factor 5. On the contrary, the density profile significantly broadens when P_{tot} increases. This appears on Fig. 10c where the evolution of the density profile parameter α_n is shown versus P_{tot}. (The approximate density profile depends on α_n by the relation $N_e = N_o(1-(r/a)^{\alpha_n})$.

Particle Confinement Time, Impurities and Edge Parameters

Fig. 12 shows, as a function of P_{tot} and at constant density n_{eo}, the behaviour of the particle confinement time τ_p, deuterium flux, impurities brilliance and concentration, Z_{eff} and the edge T_e and N_e during the power scan experiment of Fig. 9. The following observations and conclusions can be made: (i) during this power scan the total number of electrons N_e increases from 2.45 to 2.62×10^{20} particles due to profile broadening (see Figs. 9c and 12g), i.e. an increase of only ~ 7 %. As the relative increase of the deuterium fluxes at limiter $\Gamma_{D,L}$, antenna $\Gamma_{D,A}$ (Fig. 12b) and at the wall $\Gamma_{D,W}$ is much larger, the particle confinement time $\tau_p = N_e/(\Gamma_{D,L} + \Gamma_{D,A} + \Gamma_{D,W})$ degrades in a similar fashion to τ_E when P_{tot} is increased. This can be seen from Fig. 12a where $\tau_{p,OH} = 75 \pm 35$ ms. The relative increases in $\Gamma_{D,L}$, $\Gamma_{D,A}$ and $\Gamma_{D,W}$ all around the machine are roughly the same. This increase in D flux has been confirmed by a permeation probe method /28/. The dynamic time evolution at the RF switch-on or -off of these fluxes is discussed in detail in Ref. /9/. (ii) The oxygen flux increases less strongly than that of deuterium with P_{tot} /9/. This explaines the slight decrease in the oxygen concentration C_O observed from soft X-rays in Fig. 12d (assuming that the soft X-ray enhancement is only due to oxygen). The relative increases in the brilliance of OVI and CV, normalized with respect to the edge chord density at r = 40, are also slight and show roughly the same behaviour for C as for O. There is thus no low-Z impurity problem in the high power ICRH discharges with carbonized walls and C limiters. (iii) The metallic impurity behaviour, shown in Fig. 12e, is somewhat atypical in that the concentration C_{Met} (sum of Cr + Fe + Ni averaged at r=5 and 15 cm) increases more and is also larger than in other runs or earlier experiments /7,23/ due to somewhat different wall conditions. The production mechanism of these impurities is discussed in /9/. (iv) The value of Z_{eff} as given by the soft X-ray signal remains roughly constant as a function of P_{tot}; this is attributable to the combined effect of the increase in C_{Met} and decrease in C_O and C_C. (v) The evolution of the mean chord density at r = 40 cm (HCN interferometer) and the density and electron temperature measured by Langmuir probes at r=52 cm in the scrape-off layer (SOL) are shown in Figs. 12g, 12h and 12i. The increases in $n_{e,40}$ and $n_{e,52}$ are characteristic of the observed density profile broadening. The electron temperature in the SOL undergoes a mild increase during ICRH. Its possible influence on the increase of the sheath potential and resulting rise in the flux of deuterium from the wall is discussed in /9/.

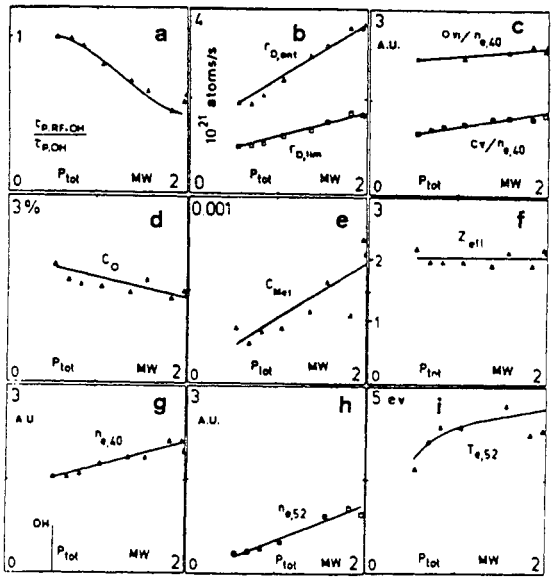

Fig. 12. Evolution of discharge parameters versus P_{tot} for the power scan experiment at constant $\bar{n}_e$ value of Fig. 9 : a) Particle confinement time τ_p ; b) Deuterium flux from main limiters and antenna limiters ; c) Impurity line brilliance normalized with respect to the edge chord density n_{e40} at r = 40 cm ; d) Oxygen concentration from soft X ray data ; e) Metallic impurities concentration from soft X-rays; f) Corresponding Z_{eff} value ; g) $n_{e,40}$; h) and i) Langmuir probe measurement of N_e and T_e at r = 52 cm in the SOL.

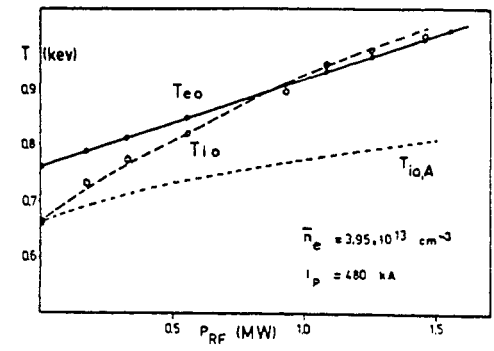

Fig. 11. Central electron and ion temperature behaviour versus P_{RF} during the power scan of Fig. 9. The dotted line gives the values of $T_{io,A}$ computed from equipartition.

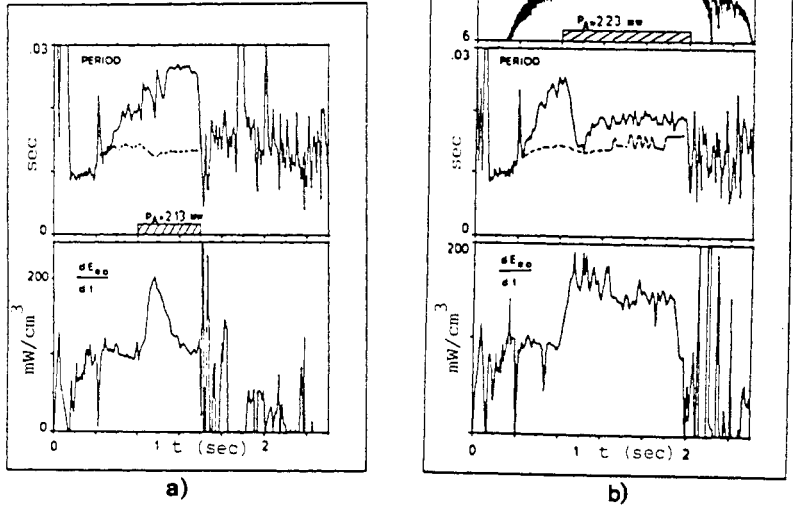

Fig. 13. Evolution of the sawteeth period and electron energy slope dE_{eo}/dt during 2 MW ICRH heated shots : a) For the shot of Fig. 8 ; b) For the shot # 20351 ; the corresponding curve of E_{eo} is also given. The dotted line gives the results of the McGuire-Robinson scaling for the period.

Fig. 15 shows the response to a given ICRH pulse (of 1.3 MW and 0.5 sec) of three different $n_e(r)$ signals, of the deuterium fluxes from limiter, antenna and liner and of the oxygen flux. These signals show as a particular feature the existence of pronounced sawteeth with amplitudes - for higher power levels - of up to 50 %. Signal b) of the lowest figure presents the local density of iron atoms in front of a non-carbonized metallic target plate which is exposed to the plasma at a radial position of r = 52.2 cm, i.e. in a position which is more than 6 cm inside the limiter shadow. The increase of the sputtered iron density there by more than one order of magnitude suggests that sufficiently energetic ions are present in this deep-shadow region. From this observation, together with the immediate onset of the effect synchroniously with the onset of ICRH, two alternative conclusions may be drawn. Either, there occurs some direct energy transfer to the ions in this region, which is not caused by the energy losses from the heated toroidal tokamak plasma flowing into the scrape-off layer: the energy decay length of about 1 cm would be too short as compared to 6 cm, the ion temperature would be too low for the measured sputtering yield and the onset of the sputtering signal would show a delay of the order τ_E. Or alternatively, the observed sputtering may be caused by high energetic trapped ions with orbits extending into this region.

Fig. 16 shows the steep increase of the density profile in the scrape-off layer (limiter radius at 46 cm) as a result of ICRH; this increase, however, is insufficient to explain the above mentioned rise of the (sputtered) iron density.

Sawtooth Behaviour during ICRH

The observation made in TEXTOR concerning the sawtooth behaviour, can be summarized as follows: 1) We observe all the variety of sawtooth behaviour already observed on other large tokamaks (e.g. /29/): single sawteeth, multiple sawteeth (up to 4 partial reconnections), sawteeth with precursors or not, sawteeth with successors or not. 2) Sawteeth on both T_{eo} and n_{eo} are contributing to the strong sawteeth on the central electron energy density E_{eo} (see e.g. Fig. 10 of /2/). The density sawteeth are mainly due to a density readjustment since the total number of particles N_e (see Fig. 8b) is only slightly affected by sawtooth behaviour at the largest ICRH power levels achieved. 3) The sawtooth period can be influenced by ICRH in different ways for roughly the same operating conditions and plasma parameters: two examples of the evolution of the period and of the mean slope dE_{eo}/dt are given in Fig. 13a (same shot as Fig. 8) and Fig. 13b. At the beginning of the RF pulse the period continues its regular increase, already started in the OH phase in Fig. 13a, whereas the period decreases strongly in Fig. 13b. At the end of the ICRH pulse, as seen in Figs. 13a and 13b, another regime of oscillation with compound sawteeth is often triggered. 4) The mean electron energy slope, during the sawtooth rise phase, decreases during the ICRH pulse. The effect of this decrease on the sawtooth amplitude is partially compensated for by a simultaneous increase in the sawtooth period (see Figs. 8c and 13b for t up to 1.4 s corresponding to the plasma current flat top). 5) The sawtooth period has been compared with the empirical scaling of McGuire and Robinson /30/. The result of this scaling is shown by the dotted line in Fig. 13a. We take a as the characteristic length and $\tau_H = (p'_{OH} + P_{RF,e})/(3/2\ n_{eo}\ T_{eo})$ as heating time, where $p'_{OH} + p_{RF,e}$ is the total power density fed to the plasma. Agreement for the order of magnitude of the period is obtained but not for the detailed behaviour.
6) Large sawteeth are also observed on the neutron yield and thus on the value of T_{io} derived from it. Fig. 14a shows a case where the value of T_{io} jumps back to the equipartition value after each internal disruption. Another case showing only a slight sawtooth behaviour is given in Fig. 14b. No general rules for the occurrence (or not) of large sawteeth have been deduced so far.

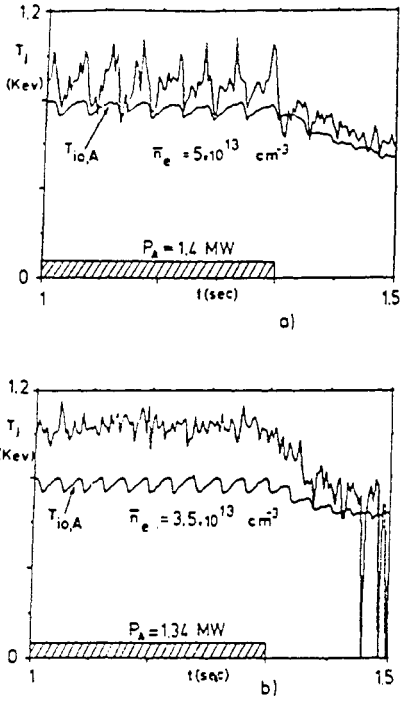

Fig. 14. Time evolution of T_{io} measured from neutrons and computed from equipartition ($T_{io,A}$) for two different shots (# 18940, 18947).

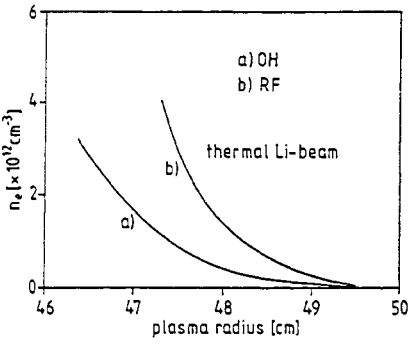

Fig. 16. Density profile in the scrape-off layer with and without ICRH (Li-beam technique).

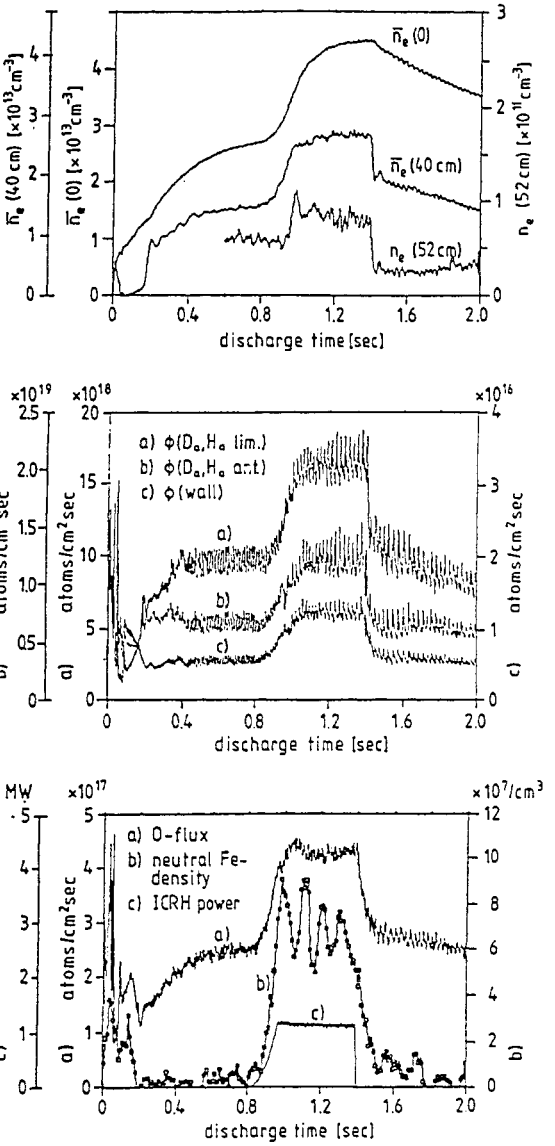

Fig. 15. Change of various $\bar{n}_e$ (r) and flux signals as a response to 1.3 MW ICRH. $\bar{n}_e$ (r) is the line averaged electron density along a chord with a distance r off the center.

	Previous Results $X_H \cong$ 5-10 %	Present Results $X_H <$ 1 %
$\Delta T_{eo}/P_{RF}$	300 eV/MW	160 eV/MW
$\Delta T_{io}/P_{RF}$	180 eV/MW	250 eV/MW
n_{eo}	3.65×10^{13} cm^{-3}	3.95×10^{13} cm^{-3}
I_p	340 kA	480 kA
$P_{RF,e}$	150-170 $\frac{mW}{cm^3 MW}$	50-60 $\frac{mW}{cm^3 MW}$
$P_{RF,i}$	60-95 $\frac{mW}{cm^3 MW}$	90-130 $\frac{mW}{cm^3 MW}$

TABLE 2 Observed central temperature increases and central power densities coupled to the elèctrons and ions per MW applied ICRH in the present experiments (with low isotope ratio $X_H = N_H/(N_H + N_D)$ as compared with the previous mode conversion experiments

SOME RESULTS OF THE PUMP LIMITER AND OF THE "ERGODIC LIMITER"

One of the focal points of the TEXTOR experimental programme is the characterization of pump limiter capabilities for particle removal as an alternative to magnetic divertors. A schematic of the modular ALT-I (Advanced Limiter Test) pump limiter /11,12,31,32/ is shown in Fig. 17 with one of the exchangeable limiter heads, the vacuum chamber (V = 700 l) and the pumping system ($S \leq 1.5 \times 10^4$ l/s).

Maximum particle removal rates of 6×10^{20} particles/s, corresponding to PxS about 10 Torr l/s (P: pressure, S: pumping speed) were achieved, enough to allow an active density control. This can be made clear by the "effective" particle confinement time τ_p^* which is the average lifetime of a particle before being either buried in the wall or pumped away. In TEXTOR, pump limiter action reduces this time from typically 2-3 seconds to 1-1.5 seconds.
The removal efficiency PxS/Q_{in} (Q_{in}: particle flux at the throat entrance) is found in the range of 0.5-1.0. Assuming $\tau_p = \tau_E$, the estimated exhaust efficiency $PxS/(Ne/\tau_p)$ results in values of up to 15 %. Please note, however, that the above mentioned maximum values of pump limiter performance were achieved by using a graphite limiter head covered with TiC-coating. The performance values of graphite limiter heads without such a coating were found to be typically a factor of 2 lower. This influence of materials on the performance may be explained by different radiation cooling layers leading to different electron temperature profiles in the boundary.

The removal efficiency can be affected by the electron temperature in the edge, with lower temperatures corresponding to higher removal rates. This observation is supported by Monte Carlo simulations of the neutral gas transport in the pump limiter /33,13/ which for an electron temperature increasing from 5 to 30 eV show a steep increase in the production rate for ion-electron pairs in the throat. In the calculations, this led to a significant attenuation of those neutrals which had a velocity component perpendicular to the magnetic field lines, and which otherwise would be carried into the pumping duct.
Three different types of pump limiter heads have been used by now. They allowed to study the effect of different geometries concerning throat lengths and both open and closed configurations /12,31,32/. From these experiments results a guiding rule for pump limiter design: the

effective pumping speed at the neutralizer plate, S_{eff}, has to be large compared to the conductance L for backstreaming of neutral gas from that region to the main plasma.

ALT-I has also been studied together with ICR heating. The power flux onto the limiter surface facing the plasma was found (infrared thermography) to increase at least as fast as the heating power P transferred to the plasma. This is a further result indicating that the ICRH power is deposited, as desired, sufficiently beyond the scrape-off layer. On the other hand, these increased power fluxes in principle have the potential to seriously affect the design and the performance of pump limiters with respect to the required shape of the leading edge in view of the tolerable heat load. However, the increase of particle fluxes and of the resulting pressure in the ALT-I chamber, which has been observed simultaneously, alleviates the above mentioned difficulty. Higher fluxes and the corresponding degradation of particle confinement time τ_p are consistent with the observations made at the main limiters mentioned earlier.
Experiments have been started to systematically evaluate the influence of the pump limiter on ICR heating ($P > 1.5$ MW), especially on energy confinement and ICRH coupling. Preliminary results indicate no improvement, but also no degradation caused by ALT-I to ICR heated discharges; within the experimental error margins both, energy confinement time and ICRH coupling remain unchanged.

"Ergodic limiters" have been proposed /14,15,34,35/ as an instrument to further reduce the particle confinement in the boundary layer, in particular to achieve some cooling effect, to enhance the fluxes into the pump limiter, and, perhaps, to obtain some impurity shielding. In summary, this method might help to approach the favourable regime of high local recycling in the boundary under non-divertor conditions.
For first experiments on this subject /16/, a localized multipolar perturbation coil has been applied on TEXTOR, accepting the disadvantage of an increased magnetic perturbation of the plasma core region as compared to large-area helical coil systems. When perturbation fields with a strength - averaged over the whole magnetic surface - of the order of 10^{-4} to 10^{-3} of the main field were applied, distinct helical structures of the boundary layer have been observed from the D_α emission there (Fig. 19). The observations confirm previous results /36/ and the explanation given there. These "optical islands" persisted also in cases where stronger perturbation fields have been applied (and a higher degree of "stochasticity" could have been expected).

Applying ergodization to pump limiter experiments, under certain conditions (island location or reduction in τ_p) the particle flux into the pump limiter throat is significantly increased, whereas also reductions have been observed in other cases.

Not only for the boundary layer but also for the core plasma rather intriguing but yet no clearcut results have been obtained at this early stage. Depending on discharge conditions in a rather subtle way, both deterioration and improvement of core confinement and of MHD mode activity could be found. In particular, in some cases a pronounced m=2 MHD mode has been observed which could be instantaneously blocked by the onset of the external perturbation fields (Fig. 20); alternatively, when the external perturbation field was ramped down, the development of such a mode has been observed.

The first experiments on the "ergodization" effects clearly demonstrated the potential of this concept to influence tokamak discharges in many respects; further investigations are necessary to obtain a more systematic picture of the induced effects in order to learn better whether or how to profit from these capabilities.

ACKNOWLEDGEMENTS

The authors would like to acknowledge the helpful support of Dr. J. Eidens in preparing the manuscript and the continuous engagement of the TEXTOR operation team in providing excellent experimental conditions.

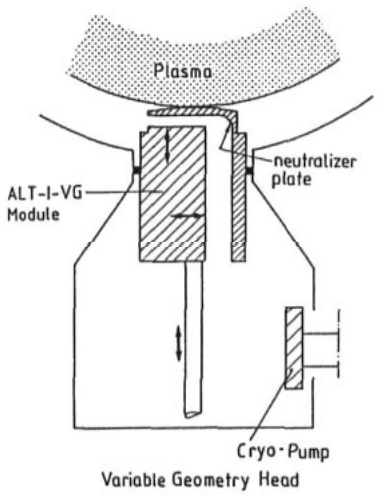

Fig. 17. Schematic view of the single head pump limiter ALT-I showing one of the various limiter heads and throat geometries. Upper surface area of limiter head ca. 30 x 30 cm^2.

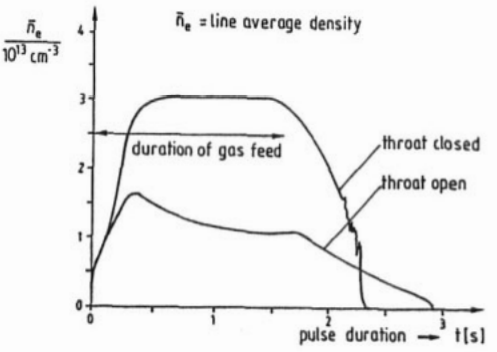

Fig. 18. Comparison of two discharges with identical gas feed, one with entrance throat closed (normal limiter operation), one with throat open (pump limiter mode).

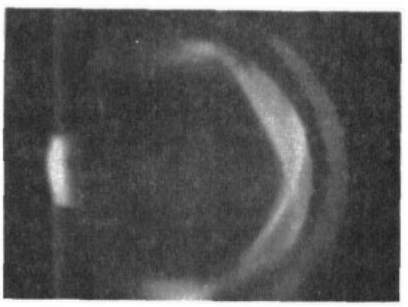

Fig. 19. Photograph in D_α light (tangential view into the torus) of the island pattern caused by the external perturbation field.

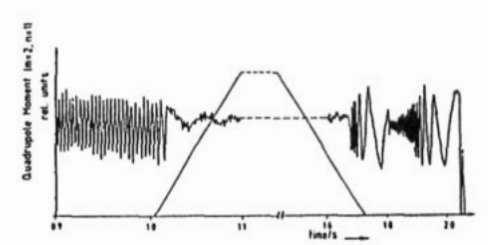

Fig. 20. Blocking of the otherwise persisting internal m = 2 modes by the external perturbation field.

REFERENCES

/1/ G.H. Wolf et al., J. Nucl. Mat. 122 & 123, 1124 (1984)
/2/ F. Waelbroeck et al., JÜL-1692 (1980)
/3/ J. Winter et al., J. Nucl. Mat. 122 & 123, 1187 (1984)
/4/ F. Waelbroeck et al., J. Nucl.Mat. 121 , 378 (1984)
/5/ J. Winter, Proc. 7th Int. Conf. PSI, Princeton (May 1986)
/6/ G. Fuchs, G. Waidmann et al., Proc. 13th Eur. Conf. Contr. Fusion and Plasma Heating, Schliersee (1986)
/7/ A.M. Messiaen et al., Plasma Physics and Contr. Nucl. Fusion 28, 71 (1986)
/8/ R.R. Weynants et al., Proc. 13th Europ. Conf. Contr. Fus. and Plasma Heating, Schliersee (1986)
/9/ B. Schweer et al., Proc. 13th Europ. Conf. Contr. Fus. and Plasma Heating, Schliersee (1986)
/10/ U. Samm et al., 11th Symp. on Fusion Engineering, Austin/Tex. (Nov. 1985)
/11/ W. Bieger et al., Proc. Int. Symp. on Plasma Wall Interaction, p. 609, Jülich (1976), EUR 5782e Pergamon
/12/ A.E. Pontau et al., J. Nucl. Mat. 128 & 129, 434 (1984)
/13/ D. Reiter et al., Proc. 13th Europ. Conf. Contr. Fus. and Plasma Heating, Schliersee (1986)
/14/ W. Feneberg, G.H. Wolf, Nucl. Fus. 21, 669 (1981)
/15/ H. Belitz et al., Proc. Europ. Tok. Workshop XII/1238/82, p. 101, Schliersee (1982)
/16/ G. Fuchs et al., Proc. 13th Europ. Conf. Contr. Fus. and Plasma Heating, Schliersee (1986)
/17/ H. Soltwisch et al., Aachen (1983), Plasma Phys. and Contr. Nucl. Fusion 26, 23 (1984)
/18/ G. Waidmann et al., Nucl. Fus. Suppl., p. 193, IAEA Vienna (1985)
/19/ H. Soltwisch, W. Stodiek, A. Kaleck, J. Schlüter, Current Distribution and Magnetohydrodynamic Activity in TEXTOR Tokamak, APS Conference, San Diego (1985)
/20/ H. Soltwisch, Current Distribution Measurement in a Tokamak by FIR Polarimetry, 6th APS Topical Conf. on High Temperature Diagnostics, Hilton Head, South Carolina, March 9-13, 1986 (to appear in Rev. Sci. Instr. 1986)
/21/ See for instance J.A. Wesson, JET-P(85)25 Report
/22/ W. Stodiek, private communication
/23/ R.R. Weynants et al., Radiofrequency Plasma Heating (Sixth Top. Conf., Calloway Gardens, GA. 1985) AIP Conference Proceedings, New York, No. 129, p. 40 (1985)
/24/ R. Koch et al., Proc. 13th Europ. Conf. Contr. Fus. and Plasma Heating, Schliersee (1986)
/25/ W.D. Brüssau and H. Soltwisch, Real-Time Evaluation of Electron and Current Density Profile Parameters on TEXTOR, JÜL-2016 (1985)
/26/ S.M. Kaye and R.J. Goldston, Nucl. Fus. 25, 65 (1985)
/27/ F. Wagner et al., Proc. 12th Eur. Conf. on Controlled Fusion and Plasma Physics, Europhysics Conference Abstract, 9F part 1, p. 335
/28/ J. Winter et al., Frühjahrstagung DPG Stuttgart (March 1986), Verhandl. DPG (vi) 21, 57
/29/ K. McGuire et al., Proc. 12th Eur. Conf. on Controlled Fusion and Plasma Physics, Europhysics Conference Abstract, 9F part 1, p. 134
/30/ K. McGuire and D.C. Robinson, Nucl. Fus. 19, 505 (1979)
/31/ K.H. Dippel et al., Plasma Physics and Controlled Nuclear Fusion Research, I p. 249, IAEA Vienna (1985)
/32/ K.H. Dippel et al., Proc. 12th Europ. Conf. Controlled Fusion and Plasma Physics, Budapest, p. 531 (1985)
/33/ G.A. Campbell et al., UCLA-Rep. (1986), to be submitted to Ph. Rev. Let.
/34/ W. Engelhardt, W. Feneberg, J. Nucl. Mat. 76 & 77, 518 (1978)
/35/ A. Samain et al., J. Nucl. Mat. 128 & 129, 395 (1984)
/36/ N. Okyabu et al., Nucl. Fus. 25, 1684 (1985)